Available online at www.sciencedirect.com
SCIENCE DIRECT
International Journal of Heat and Fluid Flow 27 (2006) 416–423
International Journal of HEAT AND FLUID FLOW
www.elsevier.com/locate/ijhff

# POD of vorticity fields: A method for spatial characterization of coherent structures

Roi Gurka [a], Alexander Liberzon [b,*], Gad Hetsroni [c,1]

[a] Department of Mechanical and Materials Engineering, University of Western Ontario, London, Canada
[b] Institute of Environmental Engineering, ETH Zurich, CH-8093 Zurich, Switzerland
[c] Faculty of Mechanical Engineering, Technion, Haifa 32000, Israel

Received 4 January 2005; received in revised form 23 December 2005; accepted 10 January 2006
Available online 6 March 2006

**Abstract**

We present a method to identify large scale coherent structures, in turbulent flows, and characterize them. The method is based on the linear combination of the proper orthogonal decomposition (POD) modes of vorticity. Spanwise vorticity is derived from the two-dimensional and two-component velocity fields measured by means of particle image velocimetry (PIV) in the streamwise–wall normal plane of a fully developed turbulent boundary layer in a flume. The identification method makes use of the whole data set simultaneously, through the two-point correlation tensor, providing a statistical description of the dominant coherent motions in a turbulent boundary layer. The identified pattern resembles an elongated, quasi-streamwise, vortical structure with streamwise length equal to the water height in the flume and inclined upwards in the streamwise–wall normal plane at angle of approximately 8°.


*PACS:* 47.27.Nz; 47.54.+r

*Keywords:* Boundary layer; Vorticity; Proper orthogonal decomposition; Coherent structures; Identification

## 1. Introduction

Turbulent boundary layers have been extensively investigated, since this is the place where the important phenomena of momentum and heat transfer, energy production and dissipation occur. One of the most important features in a turbulent boundary layer is the existence of coherent patterns (Kline et al., 1967; Panton, 1997). The role of coherent structures in the aforementioned phenomena, the interaction between the structures, and their relation to the properties of a turbulent flow, remain unclear (e.g., Tsinober, 2000). There is even no general consensus about the geometry and the spatial characteristics of the coherent structures. Extensive experimental and numerical efforts were devoted to this problem during the past years (Robinson, 1991; Panton, 1997) and several models of the coherent structures were proposed, such as hairpin vortex packets (Zhou et al., 1999), horseshoe vortex (Theodorsen, 1952), funnel (Kaftori et al., 1994), and near-wall longitudinal vortices (Schoppa and Hussain, 2000), among others. Despite their different names, the spatial characteristics of the structures in all these models exhibit a remarkable similarity. For example, the individual coherent structures in the numerical simulations (e.g., Zhou et al., 1999) were found to grow upwards in the streamwise–wall normal plane at the angle of 8–12°, as it was observed in the experiments of Head and Bandyopadhyay (1981) and Kaftori et al. (1994).

A study of coherent structures demands an objective, unbiased, statistical method of identification of the coher-

* Corresponding author.
*E-mail addresses:* rgurka@eng.uwo.ca (R. Gurka), liberzon@ihw.baug.ethz.ch (A. Liberzon), hetsroni@tx.technion.ac.il (G. Hetsroni).
[1] Tel.: +972 4 829 2058; fax: +972 48 23 8101.

0142-727X/$ - see front matter © 2006 Elsevier Inc. All rights reserved.
doi:10.1016/j.ijheatfluidflow.2006.01.001

ent patterns in the multi-dimensional data sets. Numerous identification techniques have been proposed and implemented to the results of numerical simulations and experiments (see, for example Bonnet et al., 1998). The identification methods are associated with one of the physically meaningful flow quantities, such as turbulent velocity or velocity derivatives. Vorticity, which plays a dominant role in the dynamics of turbulent flows (e.g., Klewicki, 1997; Tsinober, 2000), and linked directly to the coherent structures, is also one of the best choices for the identification (Bonnet et al., 1998; Gunes and Rist, 2004). We proposed in Liberzon et al. (2005) to use the linear combination of the proper orthogonal decomposition (Lumley, 1970) modes of the numerically simulated three-dimensional vorticity fields in order to identify and characterize the coherent structures in a turbulent channel flow. This method is distinct from the previous studies of the proper orthogonal decomposition (POD) (see reviews of Berkooz et al., 1993; Holmes et al., 1996), that have mostly analyzed velocity data, and have not used the combinations of POD modes in order to evaluate the spatial properties of the coherent structures.

In the present study we propose to use the same statistical, unbiased characterization method, and in addition, utilize the recent developments of the particle image velocimetry (PIV) experimental technique (Adrian, 1991; Raffel et al., 1998). PIV provides measurements of the two-dimensional, two-component velocity fields with a spatial resolution, which is sufficiently high for the estimation of the out-of-plane component of vorticity. We apply our method to the ensemble of the instantaneous two-dimensional scalar fields of spanwise vorticity, experimentally obtained in a turbulent flow in a flume. The goal is to identify the most essential features of the turbulent flow which are associated with high enstrophy, and characterize their geometry through the linear combination of the dominant POD modes.

Section 2 describes the flow facility and the PIV measuring system, along with the experimental results of the turbulent boundary layer. Section 3 is devoted to the presentation of the identification methodology and the discussion of the characterization results. Section 4 comprises of some general remarks for conclusion.

## 2. The experiment

### 2.1. Experimental setup

The experiment was performed in a flume with dimensions of $4.9 \times 0.3 \times 0.1$ m, shown in Fig. 1. A detailed description of the flume is given in Liberzon et al. (2003) and Gurka et al. (2004), and here it is described only briefly. The entrance and the following part of the flume (up to 2.8 m downstream) are made of glass in order to make flow visualization and PIV measurements possible. All necessary precautions were taken to reproduce the same experimental conditions as in Hetsroni et al. (1997): (i) the eddies and recirculating currents were damped by means of grids in the inlet tank (as presented by dashed lines in Fig. 1), (ii) baffles were installed in the pipe portion of the tank, the inlet to the channel was a converging channel in order to have a smooth entrance, and (iii) the pump was isolated from the system by means of rubber joints fitted to the intake and discharge pipes. The pump was a 0.75 HP, 60 RPM centrifugal pump. Flowmeter, with an accuracy of 0.5% of the measured flow rate, continuously recorded the flow rate. In order to make the measurement area long enough and avoid the flow depth decrease at the end of the flume, an array of cylinders restricted the flow before the outlet. The measurements have been performed with treated and filtered tap water.

The PIV system, shown in Fig. 2, was composed of a double, pulsed, Nd:YAG laser (170 mJ/pulse, 15 Hz, 532 nm), optics for forming light sheet, and the CCD camera (8 bit, $1024 \times 1024$ pixels) with a recording rate of 30 frames-per-second. The camera was located 0.05 m from the side wall of the flume, normal to the laser light sheet formed in the mid-plane of the flume, measuring streamwise and wall normal components of the velocity vector. Time separation between the two laser pulses was adjusted to 3 ms according to the free-stream streamwise velocity $U_\infty = 0.21$ m/s, and 150 successive velocity realizations were measured for the total time of 10 s. The Reynolds number, based on the flow height $h = 0.08$ m and the kinematic viscosity $\nu = 0.8 \times 10^{-6}$ m$^2$/s, was 21,000. Hollow glass spherical particles with an average diameter of 11 μm, were used for seeding. The calibration procedure

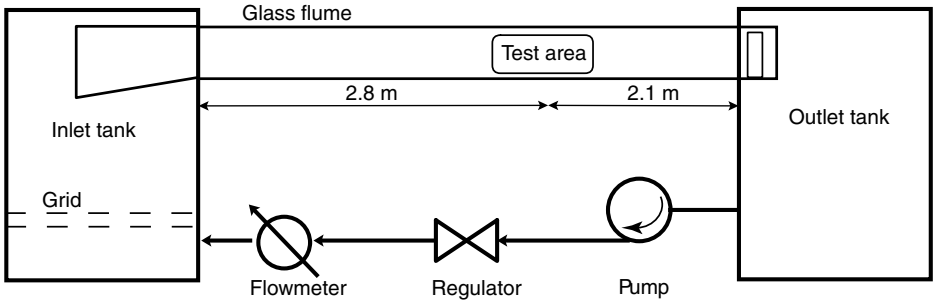


Fig. 1. Schematic view of the experimental facility.

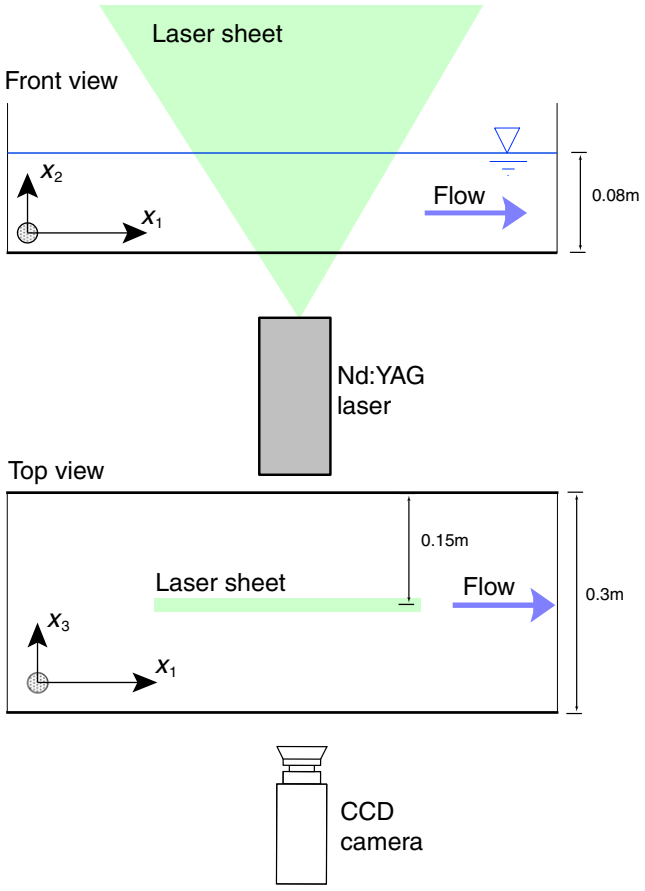


Fig. 2. Schematic drawing of the experimental setup. The measurement plane is the streamwise–wall normal plane, $x_1$–$x_2$, at the middle plane of the flume.

and PIV cross-correlation analysis were performed by using Insight 5.1 software, with $64 \times 64$ pixels interrogation areas and 50% overlapping. Spatial resolution of the camera was 80 μm per pixel which provided a field of view of approximately $80 \times 80$ mm$^2$. The analysis produced about 1000 vectors in each realization, filtered by using the standard median and global outlier filters. During the post-processing analysis, 5% of the vectors were found to be erroneous. These vectors were removed and the gaps were filled with linear interpolations of the nearest neighbor points.

### 2.2. Experimental results

We measure the two-dimensional, two-component velocity fields, $\tilde{u}_1$ $\tilde{u}_2$ in the streamwise–wall normal plane, $x_1$–$x_2$ (subscripts 1, 2 and 3 correspond to the streamwise, wall normal, and spanwise coordinates, respectively). Spanwise vorticity, $\tilde{\omega}_3$ is calculated through a numerical differentiation of the velocity fields. We denote the instantaneous fields with a tilde, ˜, the capital letters refer to the mean quantities, such as average vorticity $\Omega_3 = \overline{\tilde{\omega}_3}$, the small letters denote the fluctuating fields ($\omega_3 = \tilde{\omega}_3 - \Omega_3$), and the root-mean-square values are indicated by the apostrophe, for example $\omega_3' = \sqrt{\overline{\omega^2}}$.

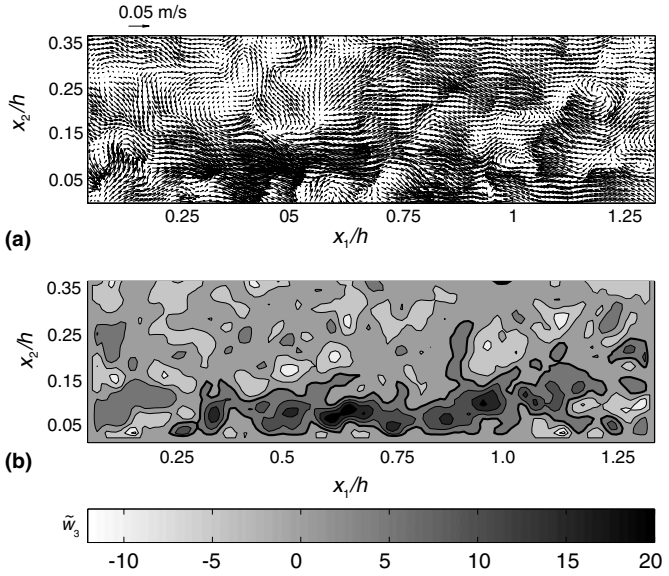


Fig. 3. Instantaneous flow field $x_1$–$x_2$ plane: (a) velocity vector field and (b) contours of the spanwise vorticity $\tilde{\omega}_3$. The flow is from left to right.

An example of the fluctuating velocity vector field $\{u_1, u_2\}$ in the streamwise–wall normal ($x_1$–$x_2$) plane is shown as a vector plot in Fig. 3a. The abscissa is the streamwise coordinate, $x_1$, and the ordinate is the wall normal normalized coordinate, $x_2$, both normalized by the water height $h$.

Despite the masking effect of the strong mean shear in the turbulent boundary layer on the underlying coherent structures, in the instantaneous fields we regularly observe the large patterns of concentrated vorticity, elongated in the streamwise direction and inclined upwards from the wall. These patterns represent, to the best of our understanding, the footprints of the large scale coherent structures, previously reported in the literature (e.g., Kaftori et al., 1994; Klewicki, 1997; Bonnet et al., 1998). An example of an instantaneous footprint of a structure could be seen in the contour plot of instantaneous vorticity field in Fig. 3b (we emphasize its envelope with a thick line).

The statistical properties of the turbulent boundary layer are given in Fig. 4. These include the profiles of the r.m.s. of velocity components, $u'$, $v'$, ($u = u_1$, $v = u_2$) the Reynolds stresses $\overline{uv}$, the mean streamwise velocity $U$ (all normalized to the free-stream velocity, $U_\infty$), and r.m.s. of spanwise vorticity $\omega_3'$, normalized by the friction velocity, $u^*$. The friction velocity $u^*$ is estimated according to Kaftori et al. (1994). The curves (1–4) (for the mean velocity and stresses) that refer to the results obtained by Klebanoff (1954) and reproduced in Schlichting (1979), are given for comparison. An additional curve (5) that shows the r.m.s. of spanwise vorticity is taken from Kim et al. (1987). Our results are presented by symbols and error bars. The symbols and the bars represent the average values and the uncertainty of the data, respectively.

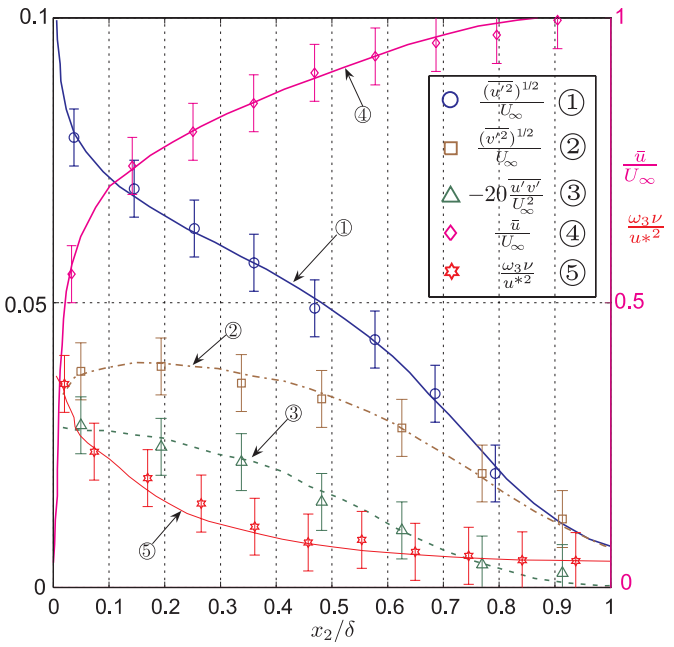


Fig. 4. Mean profiles of turbulent stresses (i.e., $u'$, $v'$, and $(\overline{uv})$), and mean streamwise velocity $U$, all normalized by the free-stream streamwise velocity, $U_\infty$, and r.m.s. of the spanwise vorticity $\omega_3'$, normalized by the friction velocity, $u^*$. Symbols and error bars represent the average and the variance of the data, respectively. For the comparison, the results of Schlichting (1979), (1–4) and of Kim et al. (1987) (5) are shown as curves.

## 3. Characterization of vorticity fields

### 3.1. Methodology

In order to insure an objective identification process, we suggested in our previous work (Liberzon et al., 2005) to adopt the following guidelines:

- Data analysis has to be performed without threshold operations, and the same filters must be applied to all the data.
- Data has to be statistically significant in order to characterize the existing structures, over a period of time.
- Analysis is based on a flow characteristic which strongly represents turbulence.

The suggested method is, in some sense, a combination of the "characteristic eddy" concept of Lumley (1970) with the reconstruction technique which is similar to one proposed by Gordeyev and Thomas (2002). The "large scale structure" or alternatively the "characteristic eddy" are identified through a linear combination of the dominant modes of the proper orthogonal decomposition (POD) of vorticity:

$$\hat{\omega}_i(x) = \sum_{n=1}^{N} a_n \phi_i^n(x) \quad i = 1, 2, 3, \tag{1}$$

where $\phi_i^n(x)$ is an eigenfunction of order $n$ of the one of the components, denoted by subscript $i$. $a_n$ denotes the corresponding coefficient. An overview of the POD procedure and the way we apply it to the PIV results are given in Appendix A.

We infer that the proposed identification method, which is defined in the above expression (Eq. (1)) and which is using the rigorously proven optimal presentation through the POD, is an objective procedure and it satisfies the guidelines listed at the beginning of this section. Moreover, we show in the following that in addition to the identification, it also provides the spatial characterization of the coherent structures in turbulent flows.

### 3.2. Characterization and discussion

The analysis, based on the POD, has been implemented in certain types of flows, such as jets, boundary layers, backward facing step flows (e.g., Holmes et al., 1996; Gordeyev and Thomas, 2002). In most of the studies the fluctuating velocity fields were analyzed, assuming that the large-scale coherent structures contain the main fraction of the turbulent kinetic energy. However, it was noted in experimental studies of Kostas et al. (2001) and Liberzon et al. (2001) and shown in our recent study of the numerically simulated flow (Liberzon et al., 2005), that the vorticity fields are more pertinent for the identification of coherent motions. This is mainly due to the fact that vorticity is Galilean invariant and, therefore, it is insensitive to the variations of the streamwise velocity that otherwise cause the so-called "jitter effect" and smear the boundaries of the coherent pattern.

We present a direct comparison of the vector POD modes of the instantaneous velocity, $\phi_{\mathbf{u}}$, with the scalar modes of spanwise vorticity, $\phi_{\omega_3}$. In order to compare the vector fields with the scalar fields, we calculate the curl of the velocity POD mode and equate it with the POD mode of spanwise vorticity. In Fig. 5a the first velocity mode is shown as a vector plot, and its curl is specified by the contour lines. There is an evidence of a large scale

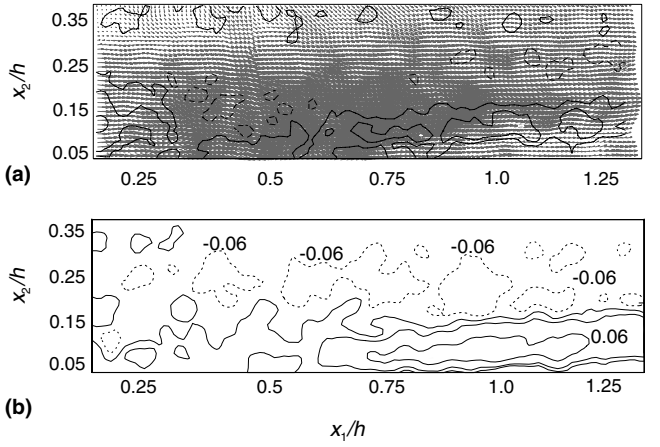


Fig. 5. (a) The vector plot of the first POD mode of the fluctuating velocity, and contour plot of the curl of the POD mode. (b) The first POD mode of the vorticity component $\phi^{(1)}(\omega_3)$.

pattern in Fig. 5a, which is elongated in the streamwise direction and inclined upwards in the streamwise–wall normal plane. We observe this pattern, more clearly in Fig. 5b, in which the boundaries of the pattern are less smeared out, it is easier identified in respect to the background vorticity and apparently also less contaminated with the noise. We infer that this is due to the weak influence of the streamwise velocity variations on vorticity, which is, by definition, a Galilean invariant.

In addition, in Fig. 6 we demonstrate that the 10 dominant POD modes of vorticity are sufficient for the reconstruction of any instantaneous vorticity field with a reasonable accuracy. The reconstruction means "partial reconstruction", defined in Appendix A (Eq. (9), $K = 10$). A relative error, based on the mean square difference between the original and the reconstructed fields, is also defined in Appendix A (Eq. (10)) and depicted in Fig. 7, along with the relative contributions of the single POD modes of spanwise vorticity. It is clear that the contribution of the first modes is much higher than of the following, higher modes, and the relative error is below 8%. We also observe that the convergence of the cumulative contribution of POD modes towards the 100% is relatively slow, as it was expected for the case of the small scale quantity, such as fluctuating vorticity (e.g., Liberzon et al., 2005).

The physical significance of vorticity in turbulent flows and the aforementioned technical details such as Galilean invariance, a sharper image and the small reconstruction error, are the main arguments for us to utilize vorticity eigenmodes in our identification method. Since a single POD mode of spanwise vorticity does not reproduce a coherent pattern typically observed in our measurements (e.g., Fig. 3b), we suggest to use the linear combination of the dominant POD modes in order to identify and characterize its spatial structure.

In Fig. 8a–c we demonstrate the linear combinations of the 3, 5, and 10 dominant POD modes of spanwise vorticity, respectively. For the sake of comparison we show the combination of all the available 150 modes in Fig. 8d. The ascertained picture in Fig. 8a–d is of the streamwise-elongated pattern of concentrated vorticity (emphasized by a thick contour line). We also realize that the shape, the streamwise length and the inclination angle of this pattern, outlined in Fig. 8a, have been not significantly altered by introducing the higher modes.

When the higher modes have been added to the linear combination, the pattern preserves its overall shape and

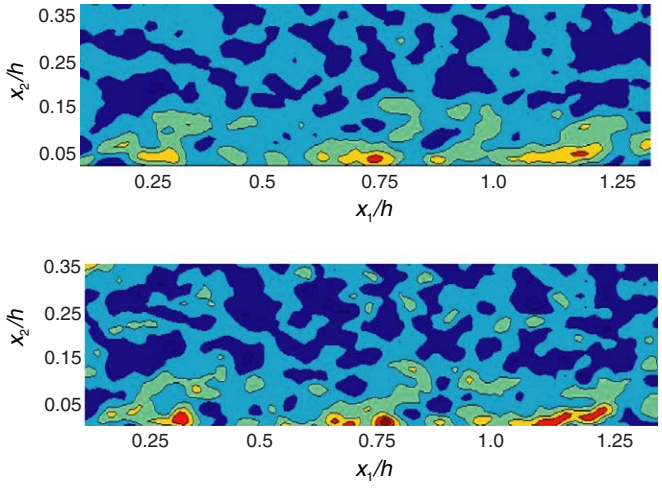


Fig. 6. Spanwise vorticity $\tilde{\omega}_3$ fields, original (top) and reconstructed by means of 10 POD modes (bottom).

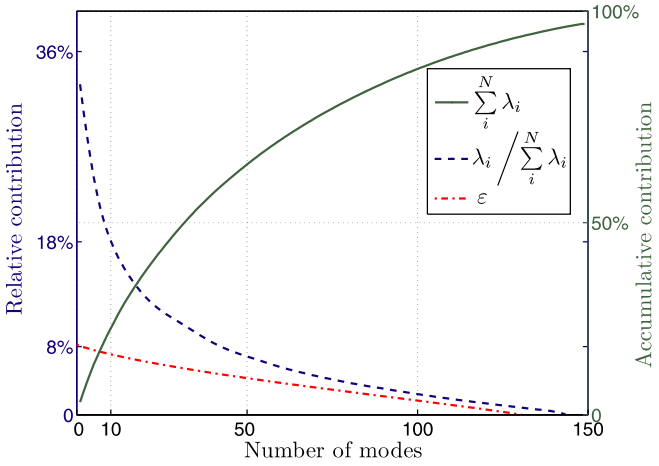


Fig. 7. Relative contribution of the single POD modes (dashed line), its cumulative summation (solid line) and relative error $\varepsilon$ (chain line), versus a number of POD modes.

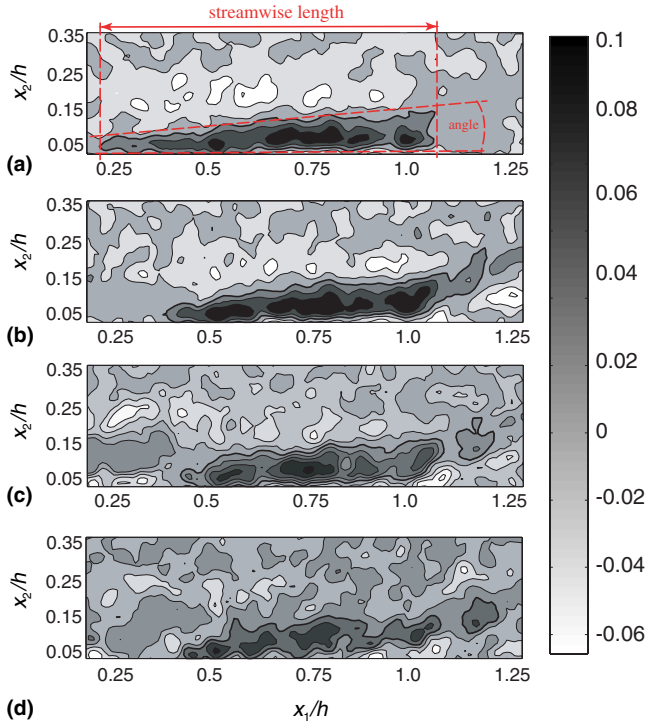


Fig. 8. Linear combination of the POD modes of the fluctuating vorticity $\omega_3$ component, (a) 3, (b) 5, (c) 10, and (d) 150 modes, respectively.

geometry, but somewhat more details have been introduced. It is possible that the small regions of high vorticity, added to the large scale pattern, for example in Fig. 8c, represent the footprints of small-scale structures (e.g., hairpins). However, since these dark zones change their shape when even more modes have been introduced, as for example in Fig. 8d, it becomes less clear if the effect is due to the small scale structures or due to the noise introduced by the PIV technique. There is a possibility that some random noise from one of the PIV components (such as CCD cameras or non-uniform particle seeding density) or a bias error in the PIV algorithm (e.g., "peak locking effect", Raffel et al., 1998) bring in the small-scale features. Experimental data with much higher spatial and temporal resolution is necessary in order to solve this ambiguity.

To summarize, we use the linear combination (defined in Eq. (1)) of the most dominant POD modes of spanwise vorticity (shown in Fig. 8a) as an identification and characterization tool that provides a qualitative information, such as the shape of the coherent structures, and the quantitative information, such as the streamwise length and the inclination angle of the coherent structures, in a turbulent boundary layer. The results shown in Fig. 8a–d emphasize the consistent spatial characteristics of the coherent patterns in the flow under investigation – the streamwise length, normalized by the water height is approximately equal to 1 and the typical inclination angle is roughly 8° in the streamwise–wall normal plane.

We can interpret the identified pattern as quasi-streamwise vortical pattern, evolving from the wall towards the outer region of the boundary layer. Keeping in mind that the measured spanwise vorticity component, $\omega_3$, is only a projection of the vorticity vector $\omega$ onto the $x_1$–$x_2$ plane, the pattern may be inferred as the footprint of an elongated quasi-streamwise vortical structure, which is growing to the sides (i.e., broadens) and upward from the wall. For example such a structure was entitled "funnel" in the experimental study of Kaftori et al. (1994), and it is also similar to the description of coherent structures disclosed by Schoppa and Hussain (2000) in a numerically simulated turbulent channel flow. The same type of the structure has been found also in our numerical investigation (Liberzon et al., 2005).

## 4. Concluding remarks

We present an experimental study of the large scale structures in a turbulent boundary layer in a flume. The two-component, two-dimensional velocity fields were measured by means of particle image velocimetry (PIV). The footprints of the coherent structures were identified and spatially characterized through the identification method, previously applied to the numerically simulated vorticity vector fields in Liberzon et al. (2005).

The method is based on the proper orthogonal decomposition (POD) of vorticity and it explicitly fulfills the proposed guidelines for any objective and statistically significant identification procedure: (i) the analysis uses an the whole data set, rather than a single flow field; (ii) it provides the spatial characteristics of a turbulent flow, on contrary to single-point statistics; (iii) it is not dependent on the choice of the basis functions (e.g., sinusoidal functions in Fourier transform, or wavelet basis), and (iv) it is based on a rigorous mathematically defined procedure of the proper orthogonal decomposition.

Based on the proposed methodology, the coherent pattern, as seen from the linear combination of the POD modes, is reflected through the spanwise vorticity component. This component is a projection of the vorticity vector, thus, we observe a footprint of an elongated quasi-streamwise vortical structure that emerge from the wall towards the mean flow and statistically have a length that is equal to the water height. The structure that we identify can be classified as a macro structure with a relative small inclination angle and is highly associated with the vorticity field. Note that the instantaneous velocity and vorticity maps do not present that feature in a repeatable manner nor does it appear in the mean values. Furthermore, decomposing the velocity fields will not yield the same result. Only by utilizing the technique on the vorticity field, a clear picture is revealed. Thus, the proposed methodology shows that coherent structures can be identified in turbulent boundary layers using two-dimensional, experimental data. In order to show a three-dimensional pattern, other fields of view in normal planes has to be measured, and three-dimensional data is necessary in order to educe the complete picture of the coherent structure. Nevertheless, the presented method, which makes use of PIV results in a single plane, gives an additional insight into the spatial structure of the flow. It has been shown to assist evaluating the low-speed streaks (see for example Gurka et al., 2004) as well as the vortical structures (Liberzon et al., 2005).

## Appendix A. Proper orthogonal decomposition (POD)

In this section the POD theory is discussed briefly and some key features of the implementation to the PIV data are presented.

POD was proposed by Lumley (1970) as an objective method to identify deterministic features in turbulent flows. The technique extracts different structures using orthogonal eigenfunctions of Karhunen–Loéve decomposition (Berkooz et al., 1993; Holmes et al., 1996). The empirical eigenfunctions are sometimes referred to as *coherent structures*, since they are highly correlated in an average sense with the flow field. In addition, the method was proved to be the optimal representation of the data (e.g., Berkooz et al., 1993).

The general goal of POD, when it is applied to some random, non-homogeneous field $f(x)$, is to find the optimally correlated feature from the given ensemble of field realizations $\{f^k\}$. The solution of the optimization problem leads to a Fredholm integral equation:

$$\int R(x,x')\phi(x')\,\mathrm{d}x' = \lambda\phi(x), \tag{2}$$

where $R(x,x')$ is the two-point correlation matrix of realizations of the random field:

$$R(x,x') = \langle f(x)f^*(x')\rangle. \tag{3}$$

The operator $\langle\cdots\rangle$ denotes ensemble average, and $*$ denotes complex conjugate. Eq. (2) has a finite set of eigenfunctions $\{\phi^n\}_{n=1}^N$ ($N$ is the length of the realization vectors), called empirical eigenfunctions, proper orthogonal modes, or eigenmodes. The whole set of the modes is a complete orthogonal set, and allows the reconstruction of any member of the ensemble $\{f^k\}$ as follows:

$$f(x) = \sum_{n=1}^{N} a_n\phi^n(x), \tag{4}$$

where $a_n$ are random uncorrelated coefficients that are square roots of the eigenvalues:

$$\langle a_n a_m^*\rangle = \begin{cases} \lambda^n & n = m, \\ 0 & \text{otherwise.} \end{cases} \tag{5}$$

The amount of random field energy could be reproduced by the sum of the eigenvalues:

$$E = (f,f) = \sum_{n=1}^{N} \lambda^n, \tag{6}$$

where the operator $(\cdot,\cdot)$ denotes the inner product

$$(f,f) = \int_x f(x)f^*(x)\,\mathrm{d}x. \tag{7}$$

Notice that in the case of the turbulent velocity field (i.e., $f(x) = u(x)$), $E$ is twice the average turbulent kinetic energy of the flow. Thus, the magnitude of the $n$th eigenvalue $\lambda^n$ represents the average kinetic energy in $n$th mode $\phi^n(x)$:

$$E^n = \frac{\lambda^n}{E}. \tag{8}$$

In the same manner, in the case of the vorticity field $f(x) = \omega(x)$, $E$ represents the average enstrophy of the flow, and each mode represents its contribution to the total enstrophy (Liberzon et al., 2005).

It is possible to represent a low order model of the random field by reconstruction on the base of $K$ dominant eigenmodes (usually the eigenvalues and eigenmodes are sorted in the ascending order $\lambda^n > \lambda^{n+1}$):

$$\hat{f}(x) = \sum_{n=1}^{K} a_n\phi^n(x). \tag{9}$$

The quality of the low-order model could be characterized by the error which is introduced by truncating the full series of the eigenmodes to the desired order. For example, we define the error of the approximation as a relative error:

$$\varepsilon = \sum_{k=1}^{N} \sqrt{\frac{|f^k(\mathbf{x}) - \hat{f}^k(\mathbf{x})|^2}{|f^k(\mathbf{x})|^2}}. \tag{10}$$

Sirovich (1987) proposed computationally efficient method of *snapshots*, which is used to compute the POD decomposition of the $M$ snapshots (realizations) of size $N$, when $M < N$, using the $M \times M$ symmetric matrix $R_{nm}$ instead of directly computed autocorrelation tensor:

$$R_{nm} = \frac{1}{M}\langle f^n \cdot f^m\rangle \quad n,m = 1\ldots M, \tag{11}$$

which eigensolutions satisfy:

$$R_{nm}\varphi = \lambda\varphi \tag{12}$$

and from which the POD modes are calculated through the projection on the original fields

$$\phi^n = \sum_{m=1}^{M} \varphi_m^n f^m, \tag{13}$$

where $\varphi_m^n$ is the $m$th element of the eigenvector $\varphi$ corresponding to the $n$th eigenvalue $\lambda^n$.

The above derivation is valid for scalar functions $f(x)$, such as the vorticity component $\omega_3$. For a vector-valued functions, such as the two-component velocity vector fields $\mathbf{u}(x) = \{u_1, u_2\}$, the tensor $R(x,x')$ is replaced by an ensemble averaged autocorrelation tensor $\mathbf{R}(x,x') = \langle \mathbf{u}(x) \otimes \mathbf{u}(x')\rangle$ and the resulting POD modes are also vector valued.

## References


Adrian, R.J., 1991. Particle-imaging techniques for experimental fluid-mechanics. Ann. Rev. Fluid Mech. 23, 261–304.

Berkooz, G., Holmes, P., Lumley, J.L., 1993. The proper orthogonal decomposition in the analysis of turbulent flows. Ann. Rev. Fluid Mech. 25, 539–576.

Bonnet, J.P., Delville, J., Glauser, M.N., Antonia, R.A., Bisset, D.K., Cole, D.K., Fiedler, H.E., Garem, J.H., Hilberg, D., Jeong, J., Kevlahan, N.K.R., Ukeiley, L.S., Vincendeau, E., 1998. Collaborative testing of eddy structure identification methods in free turbulent shear flows. Exp. Fluids 25, 197–225.

Gordeyev, S., Thomas, F., 2002. Coherent structure in the turbulent planar jet. Part 2: Structural topology via POD eigenmode projection. J. Fluid Mech. 160, 349–380.

Gunes, H., Rist, U., 2004. Proper orthogonal decomposition reconstruction of a transitional boundary layer with and without control. Phys. Fluids 16 (8), 2763–2784.

Gurka, R., Liberzon, A., Hetsroni, G., 2004. Characterization of turbulent flow in a flume with surfactant using PIV. ASME J. Fluids Eng. 126 (6), 1054–1057.

Head, M.R., Bandyopadhyay, P., 1981. New aspect of turbulent boundary layer structure. J. Fluid Mech. 107, 297–338.

Hetsroni, G., Zakin, J.L., Mosyak, A., 1997. Low-speed streaks in drag-reduced turbulent flow. Phys. Fluids 9, 2397–2404.

Holmes, P., Lumley, J.L., Berkooz, G., 1996. Turbulence, Coherent Structures, Dynamical Systems and Symmetry. Cambridge Monographs on Mechanics. Cambridge University Press, Cambridge.

Kaftori, D., Hetsroni, G., Banerjee, S., 1994. Funnel-shaped vortical structure in wall turbulence. Phys. Fluids 6, 3035–3050.

Kim, J., Moin, P., Moser, R., 1987. Turbulence statistics in fully developed channel flow at low Reynolds number. J. Fluid Mech. 177, 133–166.

Klebanoff, P.S., 1954. Characteristics of turbulence in a boundary layer with zero pressure gradient. Technical Note 1247, NACA.

Klewicki, J.C., 1997. Self-sustaining traits of near-wall motions underlying boundary layer stress transport. In: Panton (1997), pp. 135–166 (Chapter 7).

Kline, S.J., Reynolds, W.C., Schraub, F.A., Runstadler, P.W., 1967. The structure of turbulent boundary layers. J. Fluid Mech. 30, 741–773.

Kostas, J., Soria, J., Chong, M.S., 2001. PIV measurements of a backward facing step flow. In: Proc. 4th Intl. Symposium on Particle Image Velocimetry, Gottingen, Germany.

Liberzon, A., Gurka, R., Hetsroni, G., 2001. Vorticity characterization in a turbulent boundary layer using PIV and POD analysis. In: Proc. 4th Intl. Symposium on Particle Image Velocimetry, Gottingen, Germany.

Liberzon, A., Gurka, R., Hetsroni, G., 2003. XPIV – multi-plane stereoscopic particle image velocimetry. Exp. Fluids 36, 355–362.

Liberzon, A., Gurka, R., Tiselj, I., Hetsroni, G., 2005. Spatial characterization of the numerically simulated vorticity fields of a flow in a flume. Theor. Comp. Fluid Dyn. 19 (2), 115–125.

Lumley, J.L., 1970. Stochastic Tools in Turbulence. Applied Mathematics and Mechanics, vol. 12. Academic Press, New York.

Panton, R.L., 1997. Self-Sustaining Mechanisms of Wall TurbulenceAdvances in Fluid Mechanics, vol. 15. Computational Mechanics Publications, Southampton, UK.

Raffel, M., Willert, C.E., Kompenhans, J., 1998. Particle Image Velocimetry: A Practical Guide. Springer-Verlag, Berlin.

Robinson, S., 1991. Coherent motions in the turbulent boundary layer. Ann. Rev. Fluid Mech. 23, 601–639.

Schlichting, H., 1979. Boundary Layer Theory, seventh ed. McGraw-Hill, New York.

Schoppa, W., Hussain, F., 2000. Coherent structure dynamics in near-wall turbulence. Fluid Dyn Res 26, 119–139.

Sirovich, L., 1987. Turbulence and the dynamics of coherent structures. Part I: Coherent structures. Quart. Appl. Math. XLV, 561–571.

Theodorsen, T., 1952. Mechanism of turbulence. In: Proc. 2nd Midwestern Conference on Fluid Mechanics.

Tsinober, A., 2000. Vortex stretching versus production of strain/dissipation. In: Hunt, J., Vassilicos, J. (Eds.), Turbulence Structure and Vortex Dynamics, Cambridge, pp. 164–191.

Zhou, J., Adrian, R.J., Balachandar, S., Kendall, M., 1999. Mechanisms for generating coherent packets of hairpin vortices in channel flow. J. Fluid Mech. 387, 353–396.